*Journal of Fluids and Structures* (1997) **11,** 485–506

# AEROELASTICITY OF AN AIRFOIL TEST RIG

G. M. GRAHAM
*Department of Mechanical Engineering, Ohio University, Athens, OH 45701, U.S.A.*

AND

J. E. JENKINS
*2210 Eighth St., Suite 21, Wright Laboratories, WPAFB, OH 45433, U.S.A.*

(Received 18 September 1996 and in revised form 2 March 1997)

This paper describes an aeroelastic model for an airfoil test rig which is based on the mode superposition method for structural systems and linear airfoil theory for describing the unsteady airfoil loading. The model is applied to the case of an airfoil undergoing rapid, small amplitude step-like maneuvers. The motivation for these tests was an interest in measuring airfoil indicial responses, which are defined as the loading response to a step input in angle of attack. Due to the rapid starting and stopping of the airfoil rig, the structure may experience significant aeroelastic deformations. These may arise from inertial as well as aerodynamic effects. The present model may be of general interest as a means for quantifying and correcting aeroelastic effects in tow tank and wind tunnel test facilities.



## 1. INTRODUCTION

THE convolution integral formulation for the potential flow lift on a flat plate airfoil in arbitrary motion has been derived in Bisplinghoff *et al.* (1957). The formulation requires an indicial lift function which, by definition, is the transient lift response to a step change in angle of attack. The potential flow indicial lift response for a flat plate airfoil experiencing a step change in angle of attack due to plunge was first derived by Wagner (1925). Bisplinghoff *et al.* have derived Wagner's function under the assumption of small perturbations using a Fourier integral of Theodorsen's function (Theodorsen 1935) for harmonic motions. Beddoes (1984) has used the Laplace transform method to derive the lift transfer function for a number of airfoil motions. The Laplace domain formulation includes the indicial lift function. Knowledge of the indicial response is thus a central issue in modeling linear airfoil responses to arbitrary motions.

Graham *et al.* (1991) describe a tow-tank study designed to measure the normal force response of a NACA 0015 airfoil experiencing rapid step-like changes in angle of attack by rotation about the quarter chord (as measured from the airfoil leading edge). The motivation for these experiments was to study airfoil indicial-response aerodynamics as defined in the theory of nonlinear mathematical modeling for aerodynamic systems (Tobak & Schiff 1981). These experiments involved strain-gauge load-cell measurements of the transient normal force loading on an airfoil undergoing a sudden change in angle of attack of approximately $\Delta\alpha = +1°$. The angle of attack prior to the step onset ($\alpha_0$) was steady and was varied from run-to-run over the range

0889–9746/97/050485 + 22 $25.00/fl970094 

$2° < \alpha_0 < 60°$. Nonlinear mathematical modeling for aerodynamic systems extends the generality of the above linear models to account for more complex flow phenomena associated with highly unsteady motion history effects on the flow field. Such effects may include, for example, delayed flow separation due to unsteady motion, and dynamic loading augmentation associated with aerodynamic stall. From a computational standpoint, knowledge of the nonlinear indicial response is a fundamental requirement of this method.

In the present tow-tank studies, the test rig may experience large inertial and aerodynamic loading due to the rapid starting and stopping required to impart the step. Therefore, an important issue is the degree to which aeroelastic reactions deform the structure, thereby influencing the output of the strain-gauge bridge. Knowledge of these reactions is useful in comparing these strain-gauge data with the theoretical indicial response of Wagner. This paper describes an aeroelastic analysis of the Ohio University tow-tank test rig. The model is based on the mode superposition method for structural systems and classical linear airfoil theory. The Laplace transform method is used to solve the equations of aeroelasticity in closed form. The methods employed herein may be of general interest to experimentalists for quantifying the effects of aeroelasticity in tow tank and wind tunnel test rigs.

### 1.1. Ohio University Tow-Tank

A schematic of the present tow-tank is shown in Figure 1(a). The facility consists of a large tank with a 152·4 mm (6 in) chord NACA 0015 airfoil suspended vertically in the water with a submerged length of 1·067 m (42·0 in.). A carriage moves in translation at 0·61 m/s (2 ft/s) along roller bearings fixed to I-beams which span the tank. The airfoil is driven in rotation by a drive shaft fixed to the airfoil quarter chord at one end, and coupled to a 3·5 hp stepper-motor/gear-box apparatus at the other end. Figure 1(b)

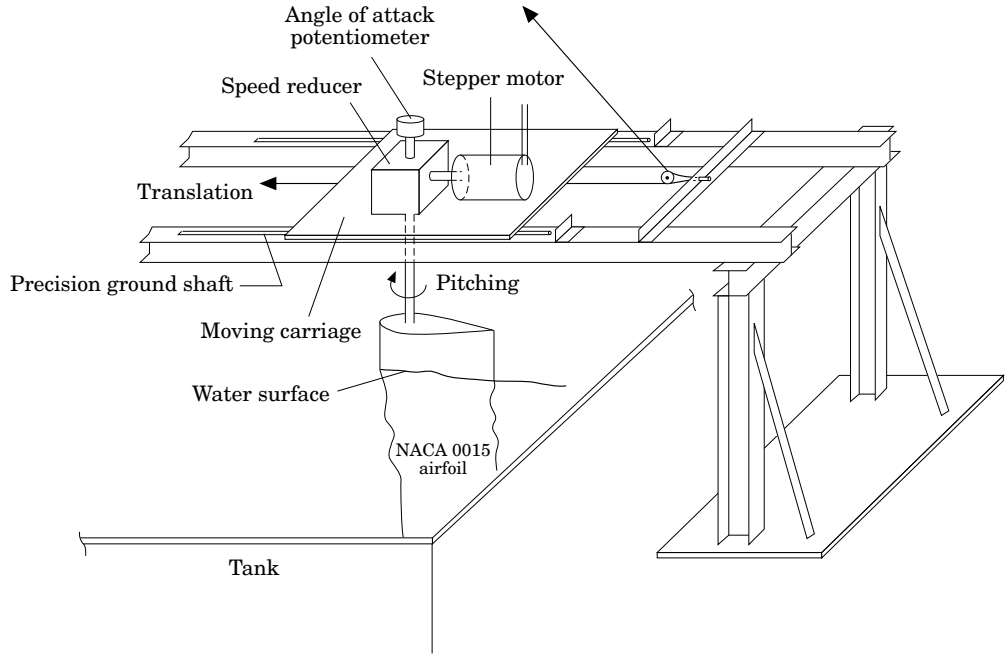


Figure 1(a). Tow-tank facility.

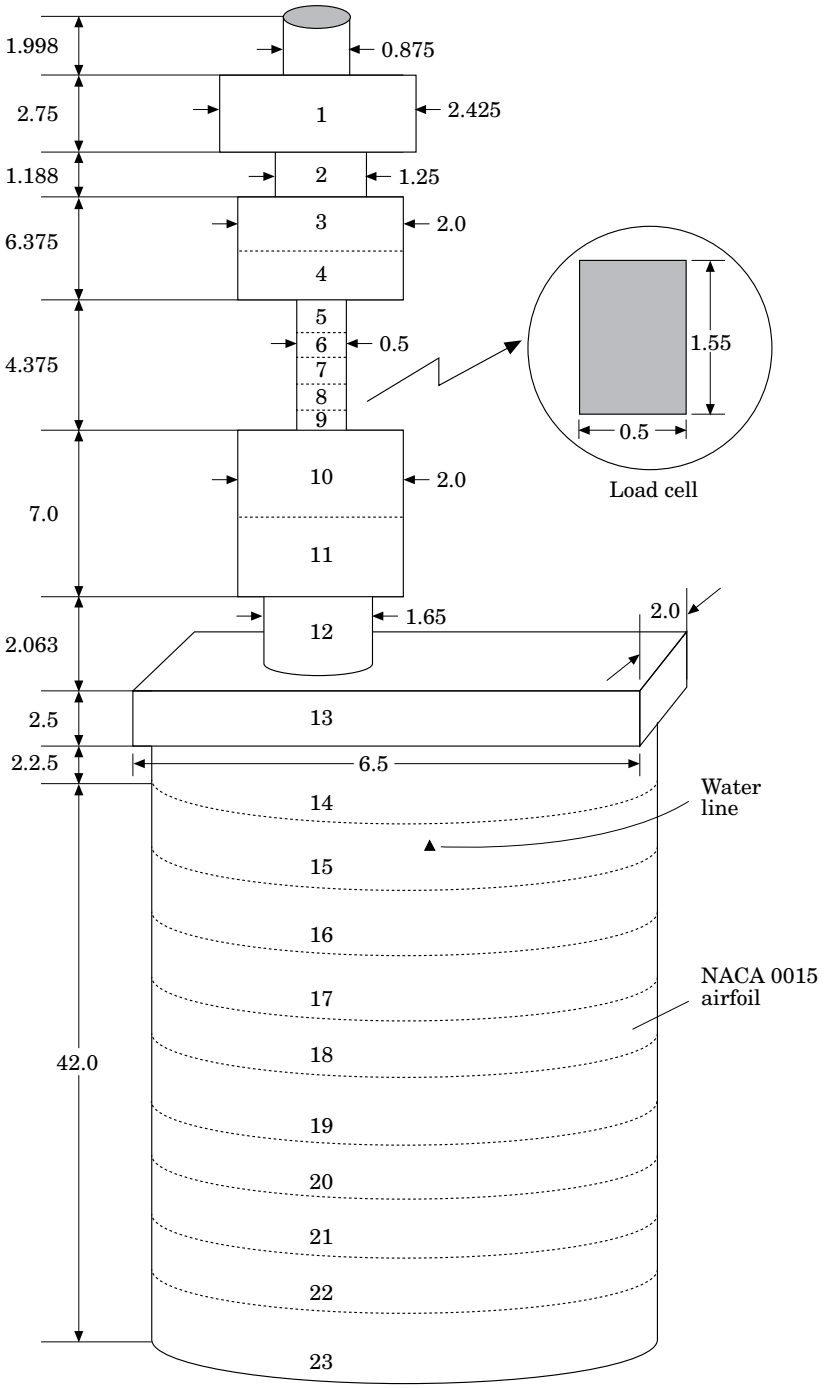


Figure 1(b). Airfoil test rig. All dimensions are in inches (1 in = 25·4 mm).

shows details of the drive shaft and airfoil. Shown here are dimensions in inches, and a numbering scheme (1–23) defined for the purpose of discretizing the mass of the structure, as will be discussed in detail. The drive shaft has a number of variations in cross-section over the length of the shaft which must be considered in modeling the

aeroelastic response of the structure. Near the middle of the drive shaft is a machined rectangular section which has a strain-gauge load-cell adhered to the shaft. The load-cell section is discretized into mass elements 5–9, with the strain-gauges located at the centroid of element 7. The strain-gauge circuit is electrically compensated to be sensitive to chord-normal forces only. The uppermost mass element 1 is made of steel, while all other parts are aluminum. The modulus of elasticity ($E$) for steel was taken to be $2{\cdot}07 \times 10^{11}\,\mathrm{N/m^2}$ ($30 \times 10^6$ psi), and for the aluminum was measured to be $5{\cdot}03 \times 10^{10}\,\mathrm{N/m^2}$ ($7{\cdot}3 \times 10^6$ psi). The modulus of rigidity ($G$) was taken to be $6{\cdot}90 \times 10^{10}\,\mathrm{N/m^2}$ ($10 \times 10^6$ psi) for the steel, and for aluminum $2{\cdot}76 \times 10^{10}\,\mathrm{N/m^2}$ ($4 \times 10^6$ psi). The area moment of inertia of the airfoil about the chord line is $4{\cdot}99\,\mathrm{cm^4}$ ($0{\cdot}12\,\mathrm{in^4}$) and the center of mass of the airfoil is located 33·31 mm (1·335 in) behind the pitch axis at the quarter chord. The polar moment of inertia of the airfoil about the pitch axis is $279{\cdot}3\,\mathrm{cm^4}$ ($6{\cdot}71\,\mathrm{in^4}$). The densities of steel and aluminum were taken to be $8{\cdot}30\,\mathrm{kg/m^3}$ and ($2{\cdot}77 \times 10^3\,\mathrm{kg/m^3}$). The mass of the airfoil per unit length is $2{\cdot}854\,\mathrm{kg/m}$ ($0{\cdot}1598\,\mathrm{lb_m/in}$).

### 1.2. Potential Flow Normal Force Response for Small Angles of Attack

In an incompressible flow at small incidence, the theoretical linear normal force coefficient response of an airfoil given an instantaneous step change in angle of attack by *rotation* about the quarter chord is related to the indicial lift function, $\Gamma(t)$, and is given by

$$C_N(t) = C_{No} + \pi\Delta\alpha[\delta(t-0) + \tfrac{1}{2}\delta(t-0)] + 2\pi\Delta\alpha[\Gamma(t) + \dot{\Gamma}(t)], \tag{1a}$$

where $C_{No}$ is the initial normal force, $\Delta\alpha$ is the step amplitude, $\dot{\delta}$ is the time derivative of the Dirac delta function $\delta$, and $\dot{\Gamma}$ is the time derivative of $\Gamma$. The first two terms in brackets in equation (1a) are generalized functions (Kaplan 1973) which describe the so-called noncirculatory component of the loading, while the last group of terms gives the circulatory component. Equation (1a) may be derived from the convolution integral formulation of Bisplinghoff *et al.* (1957) by assuming zero plunge rate and a step change in angle of attack by rotation given by $\alpha(t) = \Delta\alpha\mu(t-0)$, where $\mu(t-0)$ is the unit step function. For a flat plate airfoil the indicial function due to a step change in pure plunge can be represented by a two-pole curve fit to Wagner's function,

$$\Gamma(t) = [1 - 0{\cdot}165\mathrm{e}^{-0{\cdot}0455t} - 0{\cdot}335\mathrm{e}^{-0{\cdot}3t}]. \tag{1b}$$

Transient normal force responses of a NACA 0015 airfoil undergoing sudden step-like changes in angle of attack by rotation have been measured in the Ohio University tow-tank. Figure 2 shows angle of attack data for a typical run (small spikes are electrical noise). The onset angle is 2·09° and the step amplitude is approximately +1·25°. The motion resembles, to a reasonable approximation, a small amplitude ramp motion with a pitch rate of approximately 75°/s, which yields a nondimensional pitch rate ($\dot{\alpha}b/U$, $b$ = semichord length, $U$ = freestream velocity) of 0·16. Equation (1a) is later compared (Figure 6) with the experimental strain-gauge data corresponding to the motion of Figure 2. To facilitate the comparison, the coefficient $2\pi$ (for a flat plate airfoil) on the circulatory part in equation (1a) has been replaced by the static normal force curve slope (for the present NACA 0015) which has been measured in an independent test on the same rig. This substitution is necessary for the response of equation (1a) to approach the same steady state as the experimental response.

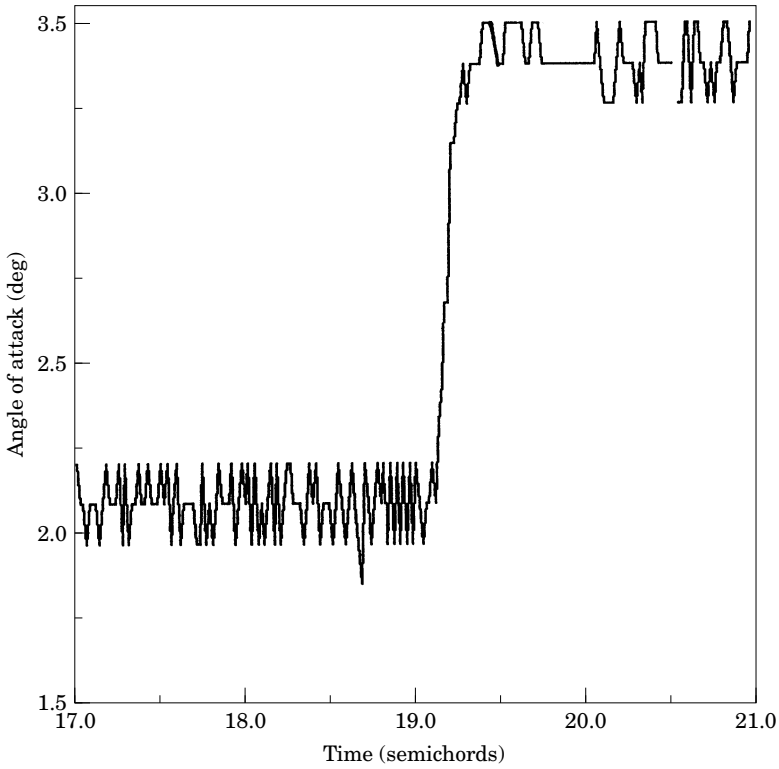


Figure 2. Angle of attack data versus time for indicial response test.

## 2. AEROELASTIC ANALYSIS

The present analysis is based on a combination of the mode superposition method for a forced structural dynamic response (Clough & Penzien 1975), and linear airfoil theory formulated in terms of the convolution integral for the loading on an airfoil in arbitrary motion (Bisplinghoff *et al.* 1957). The structure to be modeled has been shown in Figure 1(b). Because the pitch axis (drive shaft axis) does not coincide with the center of mass of the lower part of the structure (mass elements 13–23), it is necessary to consider the coupling between the normal and torsional aeroelastic degrees of freedom.

### 2.1. System Representation

As illustrated in Figure 1(b), the structure has been discretized into 23 mass elements which are considered to be concentrated at the centroid of each element. Under the influence of aeroelastic loading the masses will deflect normal to the airfoil chord, referred to here as the normal degree of freedom (NDOF), as well as in torsion about the pitch axis, hereafter referred to as the TDOF. The lowest nine masses (15–23) represent the submerged portion of the airfoil, and masses 5–9 correspond to the rectangular cross-section load-cell. Masses are concentrated on the load-cell to obtain good resolution of the deformation and strain. In the TDOF the mass elements are replaced by polar mass moment of inertia elements. For the TDOF analysis the structure is discretized in the same way as the NDOF for elements 1–12; however, elements 13–23 are lumped into a single inertia element, giving a total of 13 inertia elements. The reduction in elements in the TDOF is based on the fact that the

torsional stiffness of both the mounting block (elements 13) and airfoil are much larger than the drive shaft, and consequently the mounting block and entire airfoil experience nearly the same TDOF deflection. The resulting discretized structure may be described mathematically in terms of a diagonal mass matrix **M**, a symmetric NDOF flexibility matrix **AN**, a diagonal polar mass moment of inertia matrix **J**, and a symmetric TDOF flexibility matrix **AT**. The flexibility coefficient $AN(i, j)$ is, by definition, the deflection of mass $i$ due to a unit force applied at mass $j$, while $AT(i, j)$ gives the angular rotation of polar inertia $i$ due to a unit torque applied to inertia $j$. The matrix **AN** has been computed by assuming that the structure deforms as a cantilever beam and integrating the second order differential equation for the elastic beam curvature (Fung 1969). A condition of continuous slope is applied at discontinuities in area moment of inertia of the drive shaft. The matrix **AT** has been computed using mechanics for shafts in torsion (Higdon *et al.* 1960). The analytically derived flexibility matrices have been validated to some extent by loading the structure and measuring the deflection at selected points. For example, the analytical value of $AN(15, 15)$ is 3·4143E-3 in/$\text{lb}_\text{f}$, while the experimental value is 3·516E-3 in/$\text{lb}_\text{f}$. The NDOF stiffness matrix **KN** and TDOF stiffness matrix **KT** are computed by inverting **AN** and **AT**, respectively, and has been done using an IMSL subroutine. The structure was loaded over a wide range of loads to confirm the linearity of the stiffness in bending. The linearity of the TDOF was assumed, but not measured experimentally.

### 2.2. Eigenvalue Problem

The system matrices in the foregoing have been used to solve the eigenvalue problem for the natural frequencies and mode shape vectors of the system. The eigenvalues (natural frequencies) and eigenvectors (modal vectors) have been computed using the IMSL subroutine EVCRG. In the mode superposition analysis, the two lowest NDOF modes (NDOF1 and NDOF2) have been used, while for the TDOF only the lowest fundamental mode has been retained. The corresponding modal vectors (mode shapes) are plotted in Figure 3, where the distance from the top of the rig is measured from the top of the structure illustrated in Figure 1(b). The modal vectors are designated below as $\boldsymbol{\phi}_{N1}$, $\boldsymbol{\phi}_{N2}$ and $\boldsymbol{\phi}_{T}$ for the NDOF1, NDOF2, and TDOF, respectively.

The nondimensional natural frequencies ($\omega b/U$, $b$ = semichord length and $U$ = freestream velocity) for the NDOF modes were computed to be $\omega_{N1} = 6{\cdot}374$ (8·1 Hz) and $\omega_{N2} = 26{\cdot}985$ (34·3 Hz), and for the TDOF $\omega_T = 65{\cdot}782$ (83·8 Hz). Notice that the initial part of the angle of attack data (the ramp) of Figure 2 has a slope nearly the same as a sine function with a nondimensional frequency near 50. This frequency is, in a sense, the excitation frequency. Because the NDOF2 and TDOF natural frequencies are of the same order of magnitude as the excitation frequency, it is appropriate to consider these modal responses. As described below, the effects of apparent (added) mass are to reduce the *aeroelastic* response frequencies.

### 2.3. Structural Dynamics Model

The aeroelastic structural response of the present test rig has been modeled using the mode superposition method and classical linear airfoil theory. For modeling the rigid body rotation of the rig, a rotational degree of freedom (RDOF) is introduced. The RDOF is used to simulate the change in angle of attack of the structure due to the rotation imparted by the stepper motor. The NDOF and TDOF, as defined above,

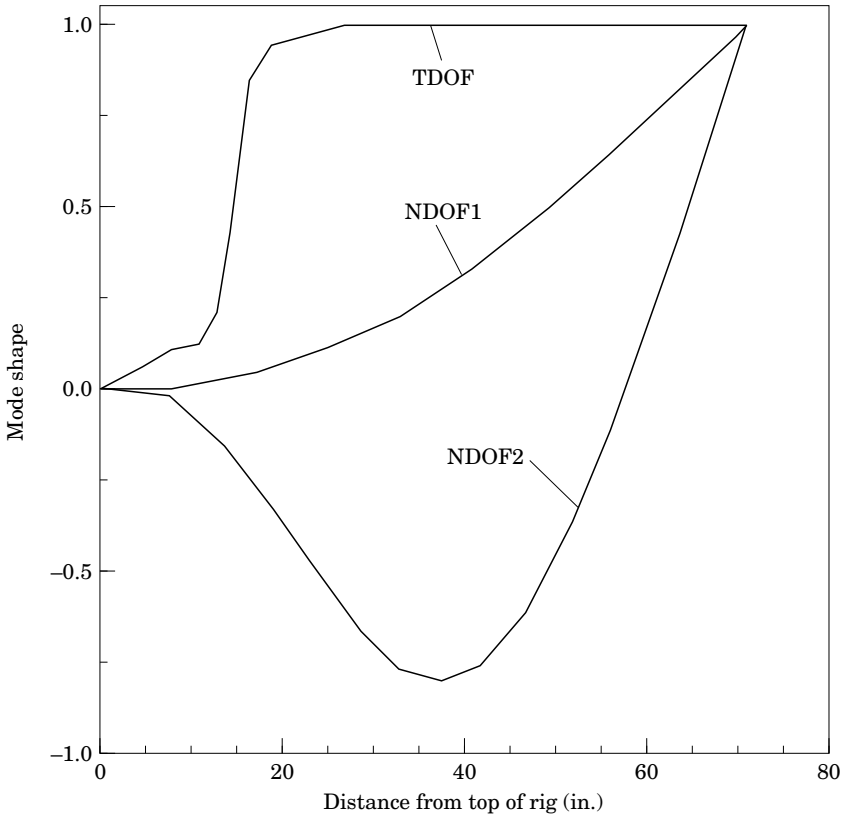


Figure 3. Modal vectors.

simulate only deformations relative to the instantaneous position of the top of the drive shaft, where both the NDOF and TDOF deflections are always zero.

In the NDOF and TDOF, the deflections of the structure are given by the normalized mode shape vectors multiplied by time-dependent modal amplitudes. The total deflection of the structure is defined by

$$\begin{aligned} \mathbf{v}_N(t) &= \boldsymbol{\phi}_{N1} q_1(t) + \boldsymbol{\phi}_{N2} q_2(t), \\ \mathbf{v}_T &= \boldsymbol{\phi}_T g(t), \\ \alpha(t) &= p(t), \end{aligned} \tag{2}$$

where $\mathbf{v}_N$ and $\mathbf{v}_T$ are the deflection vectors in the NDOF nd TDOF, respectively, and $\alpha(t)$ describes the RDOF motion. The quantities $q_1(t)$, $q_2(t)$, and $g(t)$ are the modal amplitudes and the generalized coordinates of the system. The scalar RDOF motion variable $p(t)$ is the magnitude of the nominal angle of attack as the structure is pitched, and is an input to the model. This is the angle measured by the rotational potentiometer illustrated in Figure 1(a).

Substituting equations (2) into the equations of motion for the system, and using the orthogonality of the modal vectors with respect to the system mass and stiffness

matrices to uncouple the modal equations, yields the following three generalized equations of motion:

$$\begin{aligned} M_1\ddot{q}_1 + K_1 q_1 &= \boldsymbol{\phi}_{N_1}^{\mathrm{T}}\mathbf{F}, \\ M_2\ddot{q}_2 + K_2 q_2 &= \boldsymbol{\phi}_{N2}^{\mathrm{T}}\mathbf{F}, \\ J\ddot{g} + C_T\dot{g} + K_T g &= \boldsymbol{\phi}_T^{\mathrm{T}}\mathbf{T}, \end{aligned} \tag{3}$$

where the generalized system properties are scalar quantities given by

$$\begin{gathered} M_1 = \boldsymbol{\phi}_{N1}^{\mathrm{T}}\mathbf{M}\boldsymbol{\phi}_{N1}, \qquad M_2 = \boldsymbol{\phi}_{N2}^{\mathrm{T}}\mathbf{M}\boldsymbol{\phi}_{N2}, \qquad J = \boldsymbol{\phi}_T^{\mathrm{T}}\mathbf{J}\boldsymbol{\phi}_T, \\ K_1 = \boldsymbol{\phi}_{N1}^{\mathrm{T}}\mathbf{K}\mathbf{N}\boldsymbol{\phi}_{N1}, \qquad K_2 = \boldsymbol{\phi}_{N2}^{\mathrm{T}}\mathbf{K}\mathbf{N}\boldsymbol{\phi}_{N2}, \qquad K_T = \boldsymbol{\phi}_T^{\mathrm{T}}\mathbf{K}\mathbf{T}\boldsymbol{\phi}_T, \\ C_T = 2\zeta_T J\omega_T. \end{gathered} \tag{4}$$

The damping term in the last of equations (3) is included to account for a small amount of rotational "play" in the airfoil drive shaft which tends to cause oscillations in TDOF to damp out. In equation (4), $\zeta_T$ is the damping ratio, which was estimated to be 0·05, and $\omega_T$ is the natural frequency in the TDOF. The closed form solution of equations (3) for the generalized coordiantes $q_1(t)$, $q_2(t)$, and $g(t)$, subject to a prescribed RDOF input parameter $p(t)$, is described below. Other structural models (e.g. NASTRAN) for representing the right-hand side of equations (3) are possible; however, these would have to be somehow coupled with the aerodynamic model described below, and would probably require a time-discretized numerical formulation.

### 2.4. Aeroelastic Normal Forces

The normal force acting on the structure is decomposed into a rigid body force vector, $\mathbf{F}_R$, associated with the RDOF, an aeroelastic force vector, $\mathbf{F}_A$, due to time-dependent aeroelastic deflections along the span of the airfoil, and an inertial force vector, $\mathbf{F}_I$, so that in equations (3), $\mathbf{F} = \mathbf{F}_R + \mathbf{F}_A + \mathbf{F}_I$.

The rigid-body force vector is the ideal aerodynamic loading response to a step change in angle of attack due to rotation about the quarter chord. These aerodynamic forces are exerted only on the submerged part of the airfoil represented by masses 15–23 of Figure 1(b). For a given motion input $p(t)$, the vector $\mathbf{F}_R$ at any time, $t$, at or after the step is given by

$$\begin{gathered} F_{Ri} = 0, \qquad i = 1, 2, \ldots, 14, \\ F_{Ri}(t) = \pi L_i\{\dot{p}(t) + \tfrac{1}{2}\ddot{p}(t)\} + C_{N\alpha}L_i\int_0^t [\dot{p}(\tau) + \ddot{p}(\tau)]\Gamma(t-\tau)\,\mathrm{d}\tau, \qquad i = 15, 16, \ldots, 23, \end{gathered} \tag{5}$$

where $C_{N\alpha}$ is the static normal force curve slope, $L_i$ is the span of the $i$th airfoil element, and $\Gamma(t-\tau)$ is the indicial lift response given by equation (1b). Notice that $\mathbf{F}_R$ is not a function of the generalized coordinates $q_1(t)$, $q_2(t)$ and $g(t)$, since in the ideal response the loading is given by (rigid body) 2-D airfoil theory alone. Notice also that if $p(t)$ is a unit step function of amplitude $\Delta\alpha$ and $L_i$ is unity, equation (5) becomes identical to equation (1a).

The aeroelastic force vector is also based on the convolution integral formulation for

an airfoil in arbitrary motion, and again acts only on the submerged part of the airfoil. For the pitch axis at the quarter chord the loading is

$$\begin{aligned} F_{Ai} &= 0, \qquad i = 1, 2, \ldots, 14, \\ F_{Ai}(t) &= \pi L_i\{-(\phi_{N1i}\ddot{q}_1(t) + \phi_{N2i}\ddot{q}_2(t)) + \phi_{Ti}(\dot{g}(t) + \tfrac{1}{2}\ddot{g}(t))\} \\ &\quad + C_{N\alpha}L_i\int_0^t [-(\phi_{N1i}\ddot{q}_1(\tau) + \phi_{N2i}\ddot{q}_2(\tau)) + \phi_{Ti}(\dot{g}(\tau) + \ddot{g}(\tau))]\Gamma(t-\tau)\,\mathrm{d}\tau, \\ &\qquad\qquad i = 15, 16, \ldots, 23, \end{aligned} \tag{6}$$

where $\phi_{N1i}$ and $\phi_{N2i}$ are the values of the NDOF1 and NDOF2 mode shapes at element $i$, respectively, and $\phi_{Ti}$ is the value of the TDOF mode shape. The negative sign on the NDOF terms is due to the sign convention adopted. Note that the first two terms on the right-hand side of equation (6) are the apparent mass terms, which may be combined directly with the generalized masses $M_1$ and $M_2$ in equations (3) and thus increase the ''apparent mass'' of the system. As noted below, the effect of the added mass is to reduce the aeroelastic response frequencies from the natural frequency values.

The inertial loading arises from the fact that the centroids of masses 13–23 do not coincide with the pitch axis. Thus, angular acceleration about the pitch axis produces an inertial normal force which acts at the centroid. The inertial force vector is

$$\begin{aligned} F_{Ii} &= 0, \quad i = 1, 2, \ldots, 12, \\ F_{Ii}(t) &= m_i r_i\{\phi_{Ti}\ddot{g}(t) + \ddot{p}(t)\}, \quad i = 13, 14, \ldots, 23, \end{aligned} \tag{7}$$

where $m_i$ is the mass of element $i$ and $r_i$ is the distance from the pitch axis to the centroid.

### 2.5. Aeroelastic Moments

The moments acting on the inertial elements of Figure 1(b) are also decomposed into a rigid body moment vector, $\mathbf{T}_R$, an aeroelastic moment vector, $\mathbf{T}_A$, and an inertial moment vector, $\mathbf{T}_I$, giving a total moment of: $\mathbf{T} = \mathbf{T}_R + \mathbf{T}_A + \mathbf{T}_I$. The rigid-body moment and the aeroelastic moment act only on the submerged part of the airfoil. The expressions for these components are simplified by the fact that the circulatory normal force acts at the quarter chord (for a flat-plate airfoil), giving a zero moment arm in the present study. For a NACA 0015 airfoil the circulatory normal force at a Reynolds number near $10^5$ acts within a 2% fraction of chord from the quarter chord, and on this basis has been neglected. The rigid body moment for rotation about the quarter chord is

$$\begin{aligned} T_{Ri} &= 0, \quad i = 1, 2, \ldots, 14, \\ T_{RI}(t) &= -\pi L_i\{\dot{p}(t) + \tfrac{3}{8}\ddot{p}(t)\}, \quad i = 15, 16, \ldots, 23. \end{aligned} \tag{8}$$

The aeroelastic moment vector acting on an airfoil in arbitrary motion with the pitch

axis the quarter chord is given by

$$\begin{aligned} T_{Ai} &= 0, \qquad i = 1, 2, \ldots, 14, \\ T_{Ai}(t) &= \pi L_i \{\tfrac{1}{2}(\phi_{N1i}\ddot{q}_1(t) + \phi_{N2i}\ddot{q}_2(t)) - \phi_{Ti}(\dot{g}(t) + \tfrac{3}{8}\ddot{g}(t))\}, \quad i = 15, 16, \ldots, 23. \end{aligned} \tag{9}$$

The inertial moment vector is

$$\begin{aligned} T_{Ii} &= J_i\ddot{p}(t), \qquad i = 1, 2, \ldots, 12, \\ T_{Ii}(t) &= m_i r_i[\phi_{N1i}\ddot{q}_1(t) + \phi_{N2i}\ddot{q}_2(t)] - J_i\ddot{p}(t), \qquad i = 13, 14, \ldots, 23, \end{aligned} \tag{10}$$

where $J_i$ is the mass moment of inertia of element *i*.

## 2.6. Input Rigid-Body Motion

Two input motions have been considered and are illustrated in Figure 4. The first motion is a step function input of magnitude $\Delta\alpha$, and the second input is a small amplitude ramp modeled after the experimental angle of attack of Figure 2. These motions are expressed mathematically by

$$p(t) = \Delta\alpha\mu(t - 0) \quad \text{(step)}, \tag{11a}$$

$$p(t) = \frac{\Delta\alpha}{\tau_s} t(\mu(t - 0) - \mu(t - \tau_s)) + \Delta\alpha\mu(t - \tau_s) \qquad \text{(ramp)}, \tag{11b}$$

where $\mu$ is the unit step function, and $\tau_s$ ( = 0·13 semichords) is the ramp duration, which is determined from the experimental angle-of-attack data. As will be seen, it will

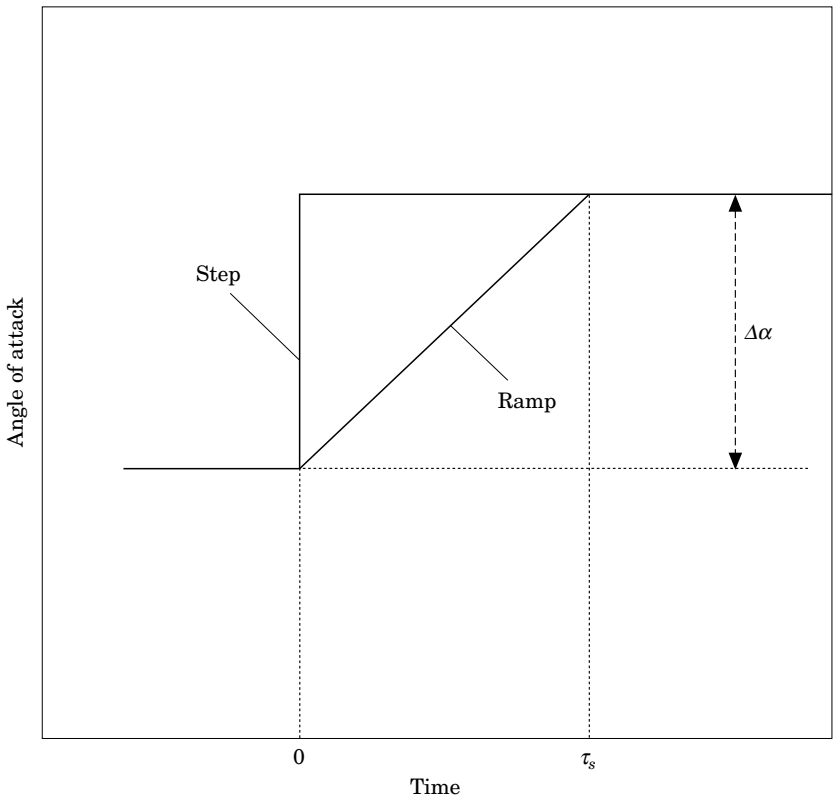


Figure 4. Step and ramp input motions.

be necessary to take the Laplace transform of equations (11a) and (11b), which yields, respectively,

$$P(s) = \frac{\Delta\alpha}{s} \quad \text{(step)}, \tag{11c}$$

$$P(s) = \frac{\Delta\alpha}{s^2\tau_s}(1 - e^{-s\tau_s}) \quad \text{(ramp)}, \tag{11d}$$

where $s$ is the Laplace variable.

### 2.7. Solution of the Generalized Equations of Motion

The Laplace transform method is used to transform the three generalized differential equations (3) into three algebraic equations which are linear in terms of the transformed generalized coordinates. These equations are solved simultaneously for the transformed generalized coordinates as functions of the Laplace variable, $s$. The inverse Laplace transform is performed to transform these solutions to the time domain to obtain $q_1(t)$, $q_2(t)$ and $g(t)$. The Laplace transform of each of equations (3) can be done by hand using standard tables. To perform the extensive algebra required in the solution, the computer program MACSYMA has been used. MACSYMA is capable of symbolic mathematics required in the solution of the simultaneous equations in terms of the Laplace variable $s$. The resulting equations of motion in the Laplace transform domain are quite long and are omitted here for brevity. Once the Laplace transforms have been done, the solution proceeds by first rearranging, using MACSYMA, the system of three equations into the following form

$$\begin{bmatrix} A_{11}(s) & A_{12}(s) & A_{13}(s) \\ A_{21}(s) & A_{22}(s) & A_{23}(s) \\ A_{31}(s) & A_{32}(s) & A_{33}(s) \end{bmatrix} \begin{Bmatrix} Q_1(s) \\ Q_2(s) \\ G(s) \end{Bmatrix} = \begin{Bmatrix} F_1(s) \\ F_2(s) \\ F_3(s) \end{Bmatrix} P(s), \tag{12}$$

where $Q_1(s)$ is the Laplace transform of $q_1(t)$, $Q_2(s)$ of $q_2(t)$, and $G(s)$ of $g(t)$. In equation (12), $P(s)$ is the Laplace transform of the motion input parameter $p(t)$ [equations (11)]. Equation (12) can be solved using Cramer's rule to yield

$$\mathbf{X}(s) = \mathbf{R}(s)P(s), \tag{13a}$$

where $\mathbf{X}(s)$ is a $3 \times 1$ vector given by

$$\{X(s)\} = \begin{Bmatrix} Q_1(s) \\ Q_2(s) \\ G(s) \end{Bmatrix}, \tag{13b}$$

and the $3 \times 1$ vector $\mathbf{R}(s)$ is an aeroelastic transfer function which is a function of the Laplace variable $s$ only, and is given by

$$R_1(s) = \frac{\begin{vmatrix} F_1(s) & A_{12}(s) & A_{13}(s) \\ F_2(s) & A_{22}(s) & A_{23}(s) \\ F_3(s) & A_{32}(s) & A_{33}(s) \end{vmatrix}}{\begin{vmatrix} A_{11}(s) & A_{12}(s) & A_{13}(s) \\ A_{21}(s) & A_{22}(s) & A_{23}(s) \\ A_{31}(s) & A_{32}(s) & A_{33}(s) \end{vmatrix}}, \quad R_2(s) = \frac{\begin{vmatrix} A_{11}(s) & F_1(s) & A_{13}(s) \\ A_{21}(s) & F_2(s) & A_{23}(s) \\ A_{31}(s) & F_3(s) & A_{33}(s) \end{vmatrix}}{\begin{vmatrix} A_{11}(s) & A_{12}(s) & A_{13}(s) \\ A_{21}(s) & A_{22}(s) & A_{23}(s) \\ A_{31}(s) & A_{32}(s) & A_{33}(s) \end{vmatrix}},$$

$$R_3(s) = \frac{\begin{vmatrix} A_{11}(s) & A_{12}(s) & F_1(s) \\ A_{21}(s) & A_{22}(s) & F_2(s) \\ A_{31}(s) & A_{32}(s) & F_3(s) \end{vmatrix}}{\begin{vmatrix} A_{11}(s) & A_{12}(s) & A_{13}(s) \\ A_{21}(s) & A_{22}(s) & A_{23}(s) \\ A_{31}(s) & A_{32}(s) & A_{33}(s) \end{vmatrix}},$$

with the brackets indicating the determinant. It is recommended that the necessary algebra be performed on equation (12) so that $R_1(s)$, $R_2(s)$, and $R_3(s)$ are the form of the quotients of two polynomials. This amounts to manipulating equation (12) so that all of the terms in the square matrix **A** and the terms in the vector **F** are at most polynomials (i.e. not themselves quotients). By way of example, the Laplace transform of the indicial function $\Gamma(t-\tau)$ will be in the form of a quotient which will initially appear in both **A** and **F**. From equation (1b), the indicial function is of the form $\Gamma(t) = 1 - A\mathrm{e}^{at} - B\mathrm{e}^{bt}$, which has a Laplace transform:

$$\gamma(s) = \frac{1}{s} - \frac{A}{s-a} - \frac{B}{s-b} = \frac{(1-A-B)s^2 + (Ab + Ba - a - b)s + ab}{s(s-a)(s-b)}. \tag{13c}$$

The quotient may be eliminated by simply multiplying the entire system of equations (12) by the denominator of $\gamma(s)$. This will render the terms of **A** and **F** as nonquotients and simplify the partial fraction decomposition which follows.

Substitution of a particular input motion, $P(s)$, into equation (12) gives the solution for the generalized coordinates in the Laplace domain. For the step input of equation (11c), the result for each generalized coordinate is in the form of a quotient of two polynomials in $s$, wherein the numerator is a 10th-order polynomial and the denominator is an 11th-order polynomial. For the ramp motion of equation (11d) the result is a 10th-order divided by a 12th-order polynomial.

In either case, the inverse Laplace transform is accomplished by decomposing the quotients using partial fractions into functions which can be inverted by hand. In the partial fraction decomposition, MACSYMA has been used to find the roots of the polynomial in the denominator. In the step input case the denominator has five real roots, while in the ramp input the denomination has six real roots with a repeated root at $s = 0$. These roots arise from the exponential terms in the indicial response function, $\Gamma$. In both the step and ramp input cases, the denominator further has three pairs of complex conjugate roots which represent the oscillatory (harmonic) response of the structure at the three frequencies associated with the NDOF1, NDOF2, and TDOF. The numerical values of the frequencies of the harmonic response can be traced to the mass (including apparent mass) and stiffness terms in the governing aeroelastic equations. The set of simultaneous equations for the undetermined constants in the expansion terms have been solved using direct factorization with maximal column pivoting (Burden *et al.* 1980). Pivoting is recommended, since the coefficients in the simultaneous equations vary over several orders of magnitude.

It is worth noting that in the ramp motion input case it is not necessary to use the full form of $P(s)$ as given by equation (11d). This is because the last exponential term on the right-hand side results in an inverse transform identical to the inverse transform of the term which precedes it, only shifted in time by an amount $\tau_s$. Thus, it is only necessary to use $P(s) = \Delta\alpha/s^2\tau_s$ when calculating this case. This effect can be seen in the solution given below.

The solutions for the generalized coordinates $q_1(t)$, $q_2(t)$ and $g(t)$ for the step input case can be represented generally by the function $f(t)$, which has the following form

$$f(t) = A + B\mathrm{e}^{bt} + C\mathrm{e}^{ct} + D\mathrm{e}^{dt} + F\mathrm{r}^{ft} + \mathrm{e}^{ht}(G\cos\omega_1 t + H\sin\omega_1 t) + \mathrm{e}^{jt}(J\cos\omega_2 t + K\sin\omega_2 t) + \mathrm{e}^{mt}(M\cos\omega_3 t + N\sin\omega_3 t), \quad (14a)$$

where each of the constants $A$ through $N$, $b$ through $f$, and $\omega_1$, $\omega_2$, and $\omega_3$ are determined in the solution procedure described above. The values of the exponents in the exponential terms ($b$–$f$) may be traced directly back to the exponents in the indicial response given by equation (1b). Numerical values of the constants may be found in Graham *et al.* (1994) by the interested reader.

It is interesting to note the effects of the apparent, or added, mass on the modal response frequencies $\omega_1$ (NDOF1), $\omega_2$ (NDOF2) and $\omega_3$ (TDOF). The natural frequency of NDOF1 is 6·4 (rad/semichord), which is reduced to 2·3 by the apparent mass. Likewise, the NDOF2 frequency is reduced from 27·0 to 12·2, and the TDOF from 65·8 to 52·2. Thus, the apparent mass effects are seen to be very significant in relation to the aeroelastic response frequencies.

For the sudden ramp of equation (11b), the solutions for $q_1(t)$, $q_2(t)$, and $g(t)$ in the time domain can be represented by a function of the form:

$$f(t) - \mu(t-\tau_s)f(t-\tau_s) \qquad [\text{e.g., } q_1(t) = f(t) - \mu(t-\tau_s)f(t-\tau_s)],$$

where $\tau_s$ is the ramp duration (0·13 semichords), and $\mu(t-\tau_s)$ is the unit step function. The "shifting" in the time of the function $f(t-\tau_s)$ is due to the exponential terms in the Laplace transform of those terms containing $\mu(t-\tau_s)$ in equation (11b). In the ramp case, $f(t)$ has the form

$$f(t) = A + Et + B\mathrm{e}^{bt} + C\mathrm{e}^{ct} + D\mathrm{e}^{dt} + F\mathrm{e}^{ft} + \mathrm{e}^{ht}(G\cos\omega_1 t + H\sin\omega_1 t) + \mathrm{e}^{jt}(J\cos\omega_2 t + K\sin\omega_2 t) + \mathrm{e}^{mt}(M\cos\omega_3 t + N\sin\omega_3 t). \quad (14b)$$

Notice the ramp motion gives rise to a term proportional to time $t$. This might be expected, since the ramp motion produces an upwash at the three-quarter chord (Bisplinghoff *et al.* 1957) proportional to $t$. For times beyond $\tau_s$, this term goes to $E\tau_s$ ( = const.) to give the steady-state lift.

The above solutions are in closed form and have the mathematical properties that might be anticipated. That is, the exponential terms giving the response to a circulatory build-up in lift after the motion input, and an oscillatory component which occurs at three distinct frequencies that arise due to the modal coupling in the forcing terms on the right-hand side of equations (3). The solutions given above are plotted in Figure 5(a–c), which shows the solutions for both the step input and ramp input. The modal coupling may be observed in the frequency content of each modal solution. As might be expected, the step input tends to excite the higher frequency TDOF more than the ramp input.

### 2.8. Calculation of the Sensible Force at the Load-cell

The purpose of the present analysis is to determine the effects of aeroelasticity on the output of the strain-gauge load-cell used in the experiments described above. In these experiments the strain-gauge output is interpreted ideally as that due to a moment exerted by a normal force applied at the midspan of the submerged part of the airfoil (point loads were applied here to calibrate the strain-gauge bridge). In reality, however, this is not the case, since the strain-gauge output is determined solely by the

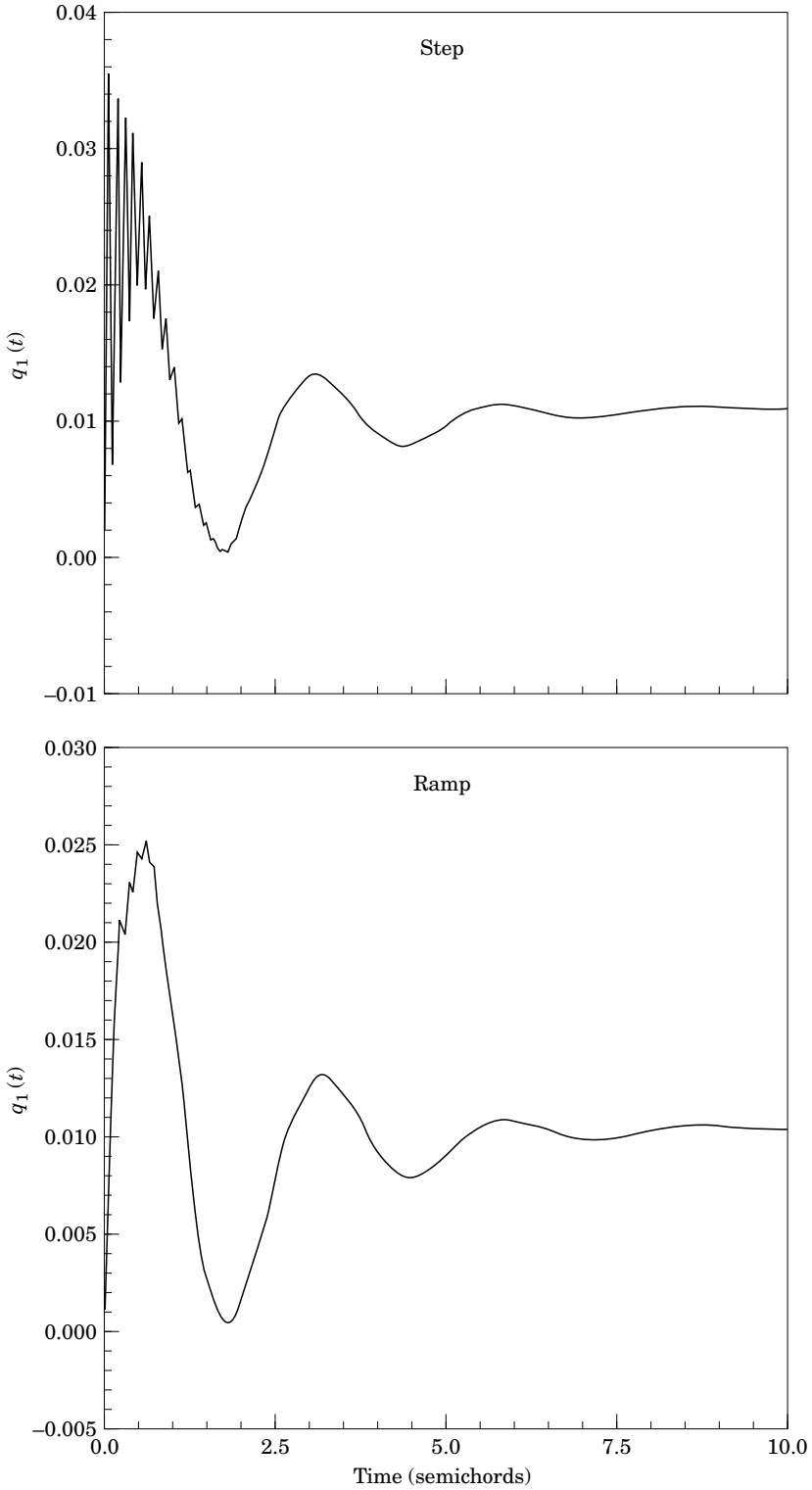


Figure 5(a). Solution for the NDOF1 generalized coordinate for step and ramp input.

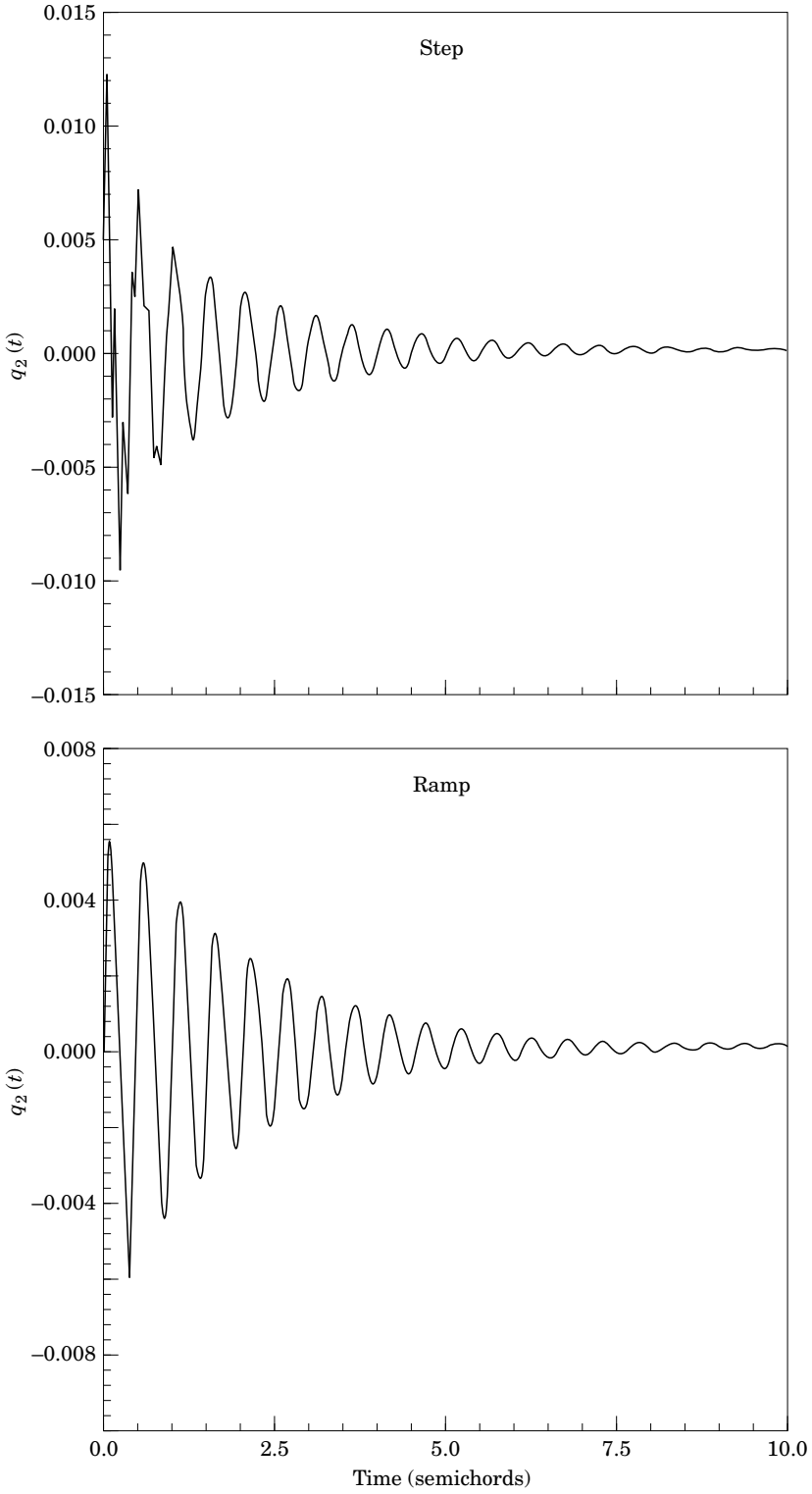


Figure 5(b). Solution for the NDOF2 generalized coordinate for step and ramp input.

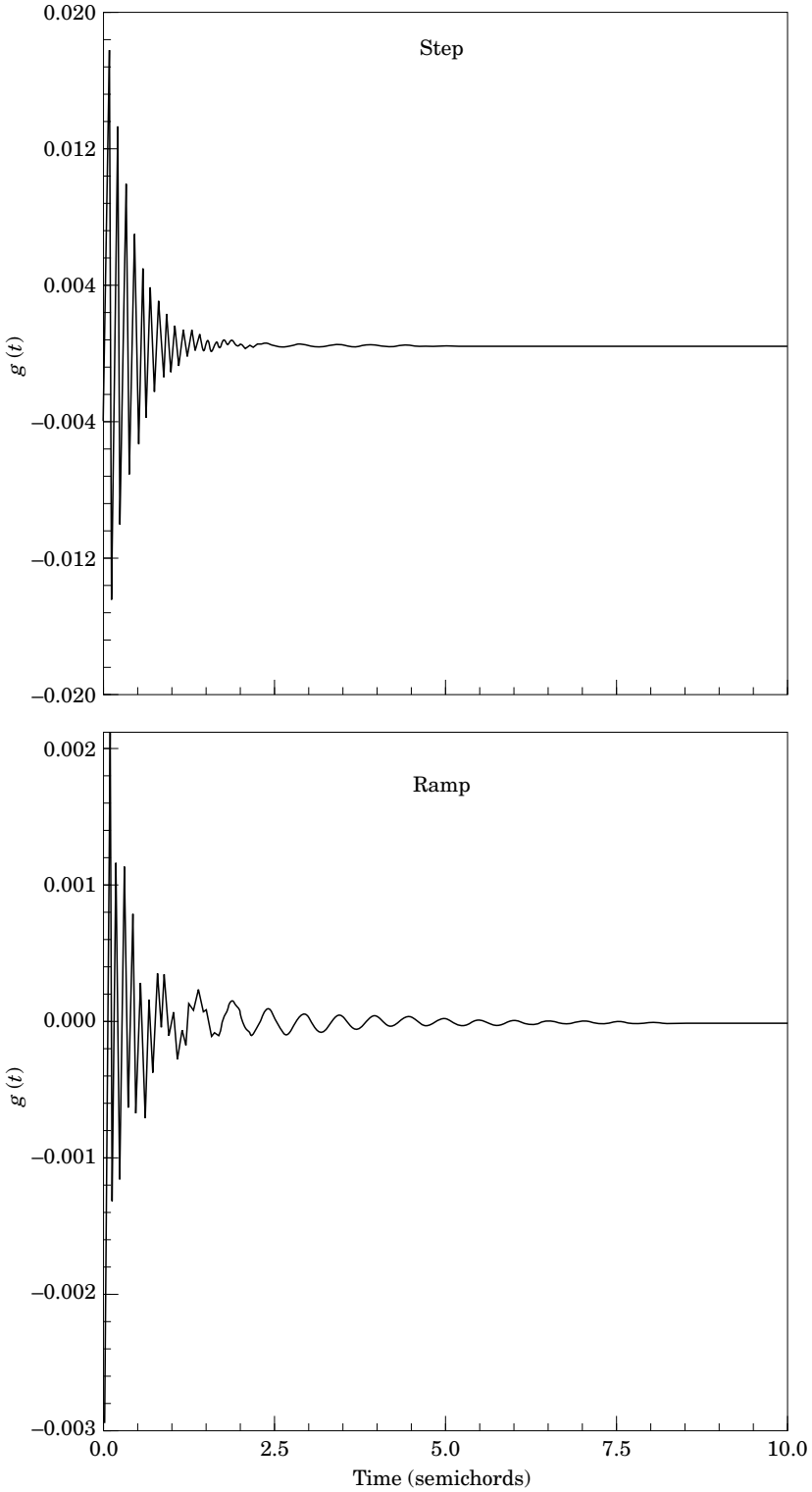


Figure 5(c). Solution for the TDOF generalized coordinate for step and ramp input.

instantaneous beam curvature at the cell. This curvature is due not to aerodynamic loading alone, but rather the total aeroelastic structural response.

From beam theory the moment at the center of the load-cell (centroid of element 7) is related to the beam curvature by

$$M_{LC}(t) = EI\left\{q_1(t)\left(\frac{\mathrm{d}^2\boldsymbol{\phi}_{N1}}{\mathrm{d}x^2}\right)_7 + q_2(t)\left(\frac{\mathrm{d}^2\boldsymbol{\phi}_{N2}}{\mathrm{d}x^2}\right)_7\right\}, \tag{15a}$$

where $x$ is measured along the span. The second derivative has been computed numerically from the NDOF mode shapes for elements 5–9 using a five-point numerical derivative given by Richardson's extrapolation method (Burden *et al.* 1980). A time-dependent "sensible" normal force acting at the midspan of the submerged portion of the airfoil which produces the same moment as that given by equation (15a) may then be defined for comparison with experimental normal force data. For this purpose, the moment arm between the mass 7 and the midspan is $L_{LC} = 37{\cdot}0$ in. These results are presented in the form of a sensible normal force coefficient, defined as

$$C_N(t) = C_{No} + \frac{M_{LC}(t)/L_{LC}}{\rho U^2 bL}, \tag{15b}$$

where $C_{No}$ is normal force at the origin of the motion, $\rho$ is the density of water, and $L$ is the submerged airfoil length (1·065 m, or 42·0 in), $U$ and $b$ are the freestream velocity and the semichord length, respectively.

## 3. RESULTS

Sensible force calculations using the present model are compared below with the experimental normal force data of Graham *et al.* (1991). A comparison is also made with recent accelerometer data taken on the Ohio University tow-tank rig undergoing the motion illustrated in Figure 2. In these tests an accelerometer (PCB Flexcel Series 336A) was placed on mass 13 (see Figure 1b) with the accelerometer centered on the pitch axis. The accelerometer is sensitive to motions in one direction only, and due to the placement of the accelerometer on the pitch axis should be sensitive to NDOF deformations only. The pitch axis of element 13 does undergo deflections in the TDOF direction; however, these are normal to the direction of sensitivity of the sensor. The accelerometer data have been integrated once and put in the form of velocity. The present model can predict velocity at any point on the structure by taking the time derivative of equations (2). The accelerometer data and normal force data below were acquired in separate runs.

### 3.1. Sensible Force and Accelerometer Comparisons

The two motion inputs given by equations (11a) and (11b) have been considered. The sensible force corresponding to the step input is compared with experimental strain-gauge data in Figure 6(a). Also shown is the theoretical response based on the Wagner function. There are three frequencies present in the aeroelastic model. The lowest frequency has a period of approximately 2·5 semichords and is associated with the NDOF1 fundamental mode. The second frequency has a period of about 0·5 semichords and is due to the NDOF2 mode, and the third highest frequency, with a period near 0·1 semichord, is due to the coupling between the TDOF and the NDOF1 and NDOF2. It is clear that aeroelastic reactions have caused significant deviation

from the theoretical response, particularly before about 2 semichords. There also is some discrepancy in the transient response at larger times.

The sensible force based on the aeroelastic response with the sudden ramp input of equation (11b) is illustrated in Figure 6(b). The response directly after the motion inception is in better agreement with the strain-gauge data than the step input results. A comparison of the aeroelastic responses of Figures 6(a) and 6(b) indicates that the step input excites the NDOF and TDOF coupling more than the sudden ramp motion, which appears to reproduce the experimental result with better accuracy. The experimental data exhibit discernible oscillations, which, in the analytical force, are associated with the NDOF2 mode. Notice from Figure 5(b) that the NDOF2 oscillations require a significant period of time to damp out. It should be noted that the uncertainty in the experimental data is near 10%.

A comparison between the aeroelastic analysis using the instantaneous step input and accelerometer data is shown in Figure 7(a). The accelerometer data have been integrated numerically and put in the form of velocity data. Again, the use of the step function input excites the TDOF mode more than the experimental data indicates. The use of the sudden ramp motion gives the results of Figure 7(b), where the agreement between the experimental data and the analysis is reasonably good.

### 3.2. Discussion

Inspection of Figure 6(b) shows some discrepancies between the experimental data and the analytical sensible force. Some potential sources of error in the present analysis are discussed below.

(i) The flexibility matrix has been derived analytically from beam theory by assuming a cantilever beam with a perfectly rigid base. In reality, however, the base may experience additional deflections, since it is mounted on slender I-beams [see Figure 1(a)] which will experience some deflection in the NDOF as the structure is loaded. The effect of this is to overestimate the structure stiffness matrix. Because the stiffness matrix is used to compute the mode shapes (eigenvectors), which are in turn used to compute the generalized properties, this will introduce errors into both the NDOF generalized stiffness and the generalized mass. Errors in the stiffness will also, of course, affect the computed natural frequencies (eigenvalues). Errors of as much as 10% are easily conceivable. This may be an important consideration in the design of dynamic test rigs.

(ii) Structural nonlinearities must also be considered. However, notwithstanding errors in flexibility discussed above, the deflection of the structure due to applied static loads has been measured over a wide range of loads at several points on the rig. These measurements have indicated, at least statically, linear stiffness.

(iii) The aerodynamic model employed herein is based on the potential flow indicial response for a flat plate airfoil. There are undoubtedly errors associated with this assumption, since the present flow is neither truly potential, nor is a NACA 0015 airfoil a flat plate. In the former case it is well known that for airfoils having even small thickness, some flow separation occurs on the aft portion of the upper surface of the airfoil even at low angles of attack. This separation is, of course, a viscous phenomenon and results in some loss of lift. In the later case, from potential flow theory, thickness adds additional lift, which for a NACA 0015 airfoil theoretically amounts to about 11% more lift. This additional potential flow lift is, however, mitigated by viscous losses. To what extent this occurs is not well known. In fact, a careful review of the literature on static airfoils reveals a significant departure from potential flow predictions [see, for

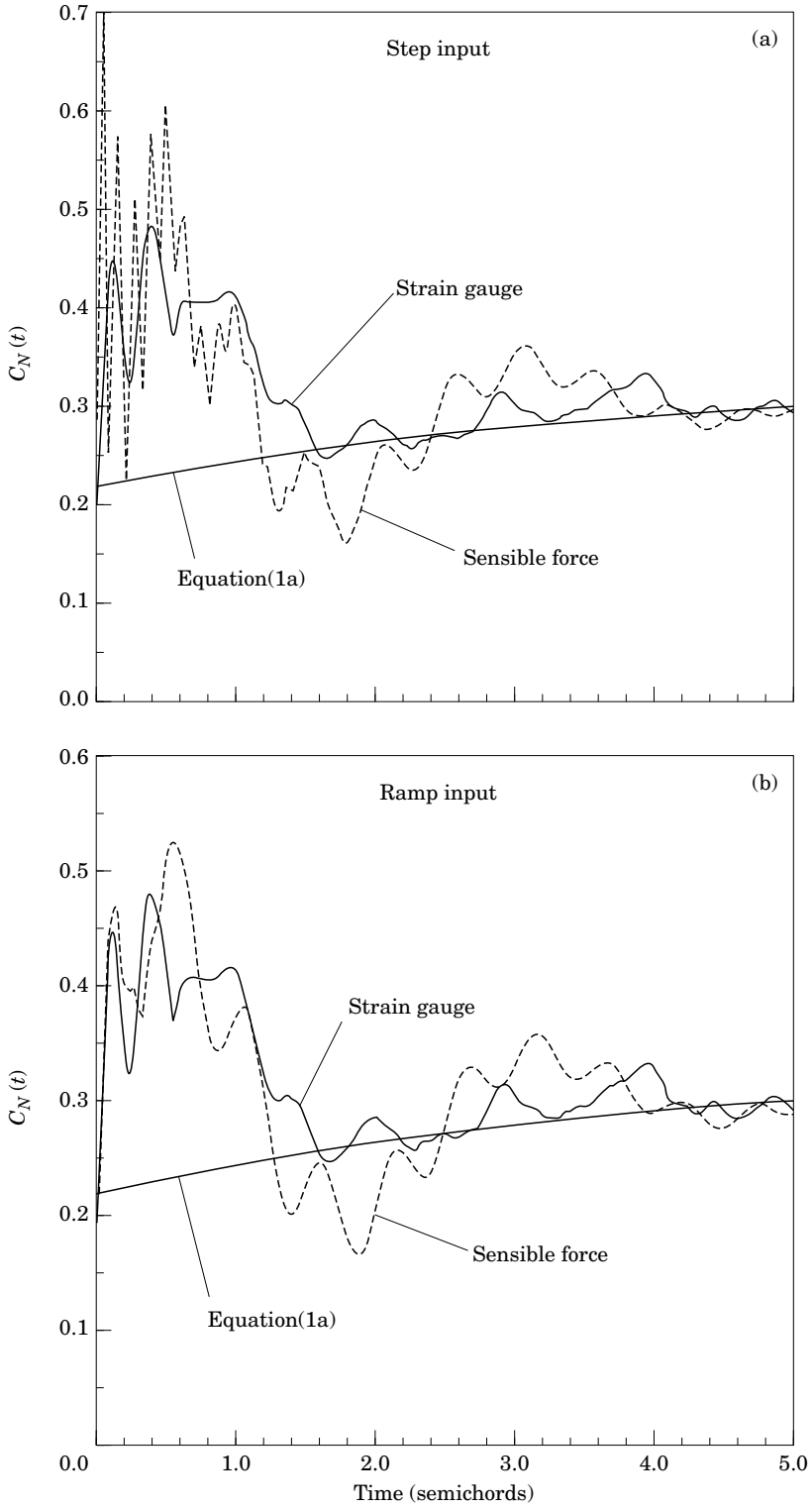


Figure 6. Sensible force at the load cell (a) for step input and (b) for ramp input.

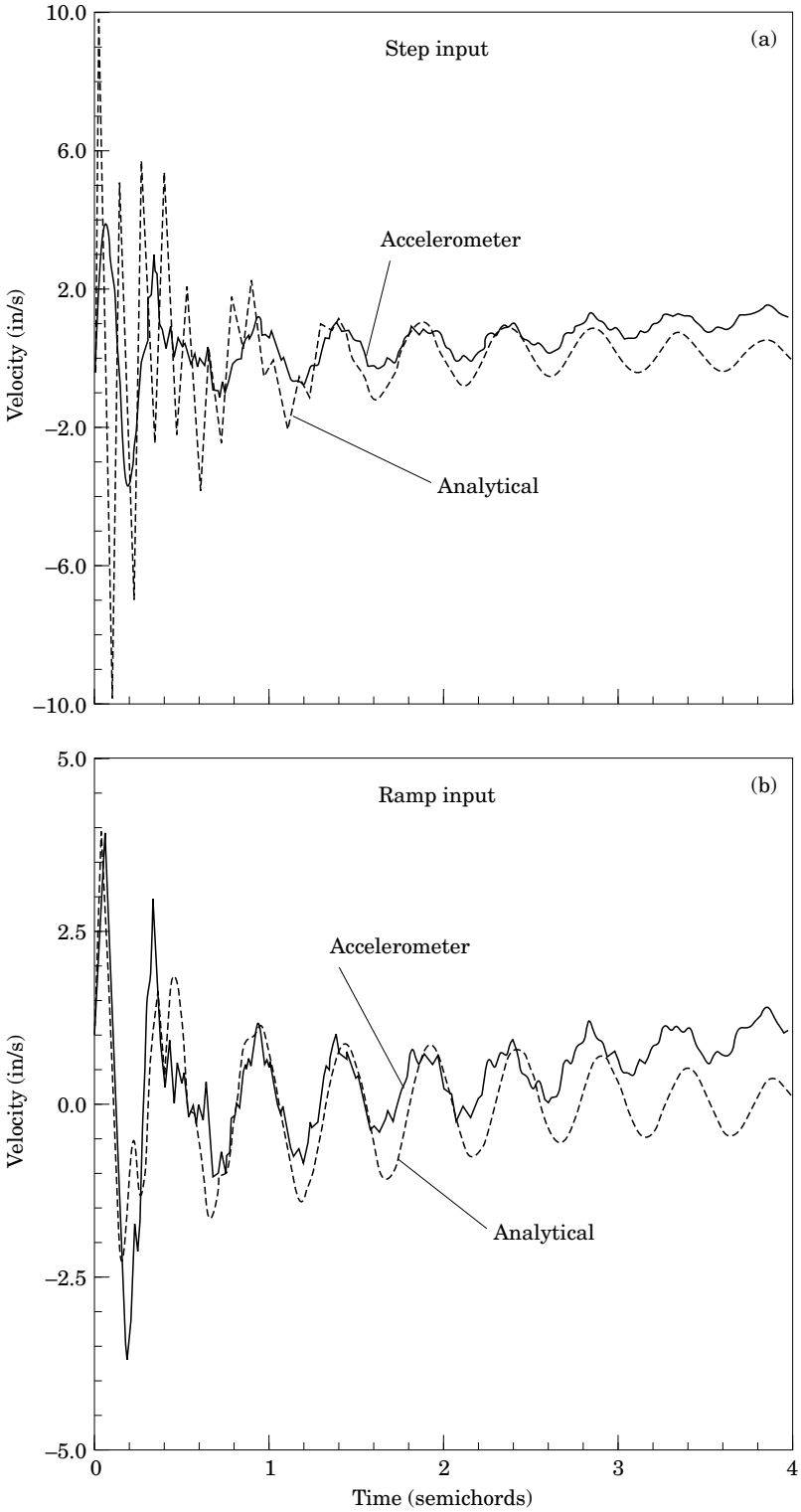


Figure 7. Velocity predictions and integrated accelerometer data for (a) step and (b) ramp input motions; 1 in/s = 25·4 mm/s.

example, the data of Jacobs & Sherman (1937)] as well as discrepancies from test facility-to-facility.

These types of phenomena will manifest themselves through the representation of the indicial response given by equation (1b), and will alter the values of the constants which appear in the equation (assuming, that is, that the mathematical form of this response remains valid). Variations in the constants 0·165 and 0·335 will alter the initial instantaneous value of the response. More importantly, perhaps, the exponents $-0{\cdot}0455$ and $-0{\cdot}3$ in the exponential terms will change the time constants of not only the indicial response, but also the time constants of the aeroelastic response. Note that in equations (14a) and (14b) the values of the exponents $b$ and $c$ have been computed to be approximately $-0{\cdot}0455$, and the constants $d$ and $f$ to be near $-0{\cdot}3$. Thus, the exponents in the indicial response naturally find their way through the analysis into the system aeroelastic response. This may be the source for some of the observed discrepancies in time of the sensible force results of Figure 6(b). The authors are unaware of an indicial response model specific to NACA series airfoils.

## 4. CONCLUSIONS

The present analysis has been conducted to determine the effect of aeroelastic reactions on airfoil indicial response tests conducted in a tow tank facility. The analysis has been validated to a reasonable level of accuracy by comparing with strain-gauge and accelerometer data. The results indicate that aeroelasticity causes significant deviation from the 2-D theoretical response shortly after the motion inception. The focus of future research will be to use the present aeroelastic model as a basis for correcting the indicial response strain-gauge data of Graham *et al.* (1991) for aeroelastic effects. In some sense, this amounts to working the present analysis in reverse. That is, in the present analysis we are given an indicial lift function, and for a given motion we compute the aeroelastic response. In the inverse problem we are given an aeroelastic response for a given motion, and we seek to compute the indicial lift function which produces the response. A theoretical method for the inverse problem has been developed by Graham & Islam (1994), and is being applied to the present tow-tank data. An alternative to this approach of correction would be to use an aeroelastic analysis in the design stage of a test rig to minimize aeroelastic contributions. The present analysis may be of general interest as a tool for quantifying these effects in wind tunnel and tow tank test facilities.

## ACKNOWLEDGEMENT

The authors gratefully acknowledge the support of the Air Force Office of Scientific Research under Grant F49620-93-0030.

## References

Beddoes, T. S. 1984 Practical computation of unsteady lift. *Vertica* **8,** 55–71.

Bisplinghoff, R. L., Ashley, H. & Halfman, R. L. 1957 *Aeroelasticity,* pp. 251–293. Reading, MA: Addison-Wesley.

Burden, R. L., Farres, J. D. & Reynolds, A. C. 1980 *Numerical Analysis,* pp. 185 and 351. Prindle, Weber, & Schmidt.

Clough, R. W. & Penzien, J. 1975 *Dynamics of Structures* pp. 176–190. New York: McGraw-Hill.

FUNG, Y. C. 1969 *An Introduction to the Theory of Aeroelasticity.* pp. 19–27. New York: Dover Publications.

GRAHAM, G. M., ISLAM, M. & JENKINS, J. E. 1991 Nonlinear normal force indicial responses for a 2-D airfoil. AIAA Paper No. AIAA-91-2866-CP.

GRAHAM, G. M. & ISLAM, M. 1994 Aeroelastic reciprocity: an indicial response formulation. Report No. AFOSR-TR-95-0700, 1995.

HIGDON, A., OLSEN, O. H., STILES, W. B., WEESE, J. A. & RILEY, W. F. 1960 *Mechanics of Materials,* pp. 182–188, 228–229. New York: Wiley and Sons.

JACOBS, E. J. & SHERMAN, A. 1937 Airfoil section characteristics as affected by variations of the Reynolds number. NACA Report 586.

KAPLAN, W. K. 1973 *Advanced Calculus* (2nd ed.), pp. 515–521. Reading, MA: Addison-Wesley.

THEODORSEN, T. 1935 General theory of aerodynamic instability and the mechanism of flutter. NACA Report 496.

TOBAK, M. & SCHIFF, L. B. 1981 Aerodynamic mathematical modeling–basic concepts. AGARD Lecture Series No. 114, Paper 1.

WAGNER, H. 1925 Über die Entstehung des dynamischen Auftriebes von Tragflügeln. *Zeitschrift für angewandte Mathematik und Physik* **5,** No. 1.